Faraday Discussions

Accepted Manuscript

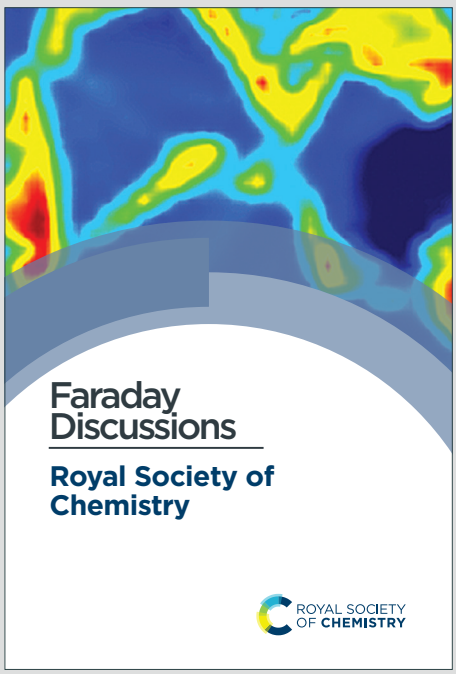

This article can be cited before page numbers have been issued, to do this please use: M. Quien, C. Ritt, S. Garimella, Z. Wei, M. T. Dronadula, N. R. Aluru and M. Strano, *Faraday Discuss.*, 2026, DOI: 10.1039/D6FD00034G.

ROYAL SOCIETY OF CHEMISTRY

www.rsc.org/faraday_d

View Article Online
DOI: 10.1039/D6FD00034G

Ambient Stability and Surface Adhesion of 2D Polyaramid NanoFilms

Michelle Quien[1], Cody L. Ritt[1], Sanjay S. Garimella[1], Zitang Wei[1], Mohan T. Dronadula,[2] Narayana R. Aluru[2], and Michael S. Strano[1]

[1]Department of Chemical Engineering, Massachusetts Institute of Technology, Cambridge, MA 02139, USA
[2]Department of Mechanical Engineering, University of Texas at Austin; Austin, Texas 78712, USA

Abstract: Two-dimensional polyaramids (2DPA) represent an emerging class of solution-synthesized, molecularly thin polymer sheets that combine the exceptional in-plane mechanical strength and barrier performance of conventional 2D materials with the synthetic versatility of organic polymers. Despite increasing interest in 2D polymers as gas barriers and membrane materials, the long-term stability of nanometer-scale suspended films remains largely unexplored. Here, we report the first longitudinal study of 2D polyaramid (2DPA-1) nanofilm bulges monitored continuously for over 1000 days. Using a microwell bulge test platform integrated with atomic force microscopy and optical interferometry, we show that 2DPA-1 forms highly stable, gas-retaining membranes whose upward deflection persists for years under ambient environmental fluctuations. Using a single-point mechanical model with thermodynamic analysis, we show that initial bulge pressurization proceeds through transient rim seal opening, while the intact seal remains robust during thermal cycling up to 120%˚C without measurable gas loss. Together, these results establish a comprehensive mechanistic framework for long-term stability, permeability assessment, and interfacial failure modes in nanofilm bulge systems. This framework enables reliable interpretation of bulge test data and provides design principles for next-generation 2D polymer membranes intended for ultrahigh-barrier, filtration, and separation technologies.

1. Introduction

Two-dimensional (2D) polymers have attracted interest in recent years as a means of combining the tools of organic chemistry with the in-plane mechanical strength and barrier properties characteristic of conventional, nominally crystalline, 2D materials.[1,2] Accordingly, 2D polyaramids (PA) have emerged as a class of 2D polymers synthesized via irreversible solution-phase polycondensation reactions with outstanding mechanical and chemical stability.[3,4] The intersection of nanoscale physics and macroscale engineering phenomena creates unique challenges in materials characterization, where traditional bulk measurement techniques fail to capture the interfacial effects that dominate nanometer thin film behavior. The microwell bulge for nanofilms is a powerful experimental platform that bridges fundamental materials science with practical engineering assessment, enabling simultaneous measurement of elastic properties,[5–8] inelastic properties,[5,9] and transport phenomena[10–12] through a unified theoretical framework. Moreover, these tests allow for sensitive measurements, such as the ultra-low impermeability of various two-dimensional (2D) materials,[4,10,13,14] which are not possible in the equivalent macroscale experiment. Herein, we detail an unprecedented longitudinal study of 2D polyaramid nanofilm bulges that have persisted as inflated for more than 1000 days. This prolonged study enables the mechanistic elucidation of factors that influence bulge metrics (e.g., deflection) and, consequently, gas permeability and mechanical measurements. Specifically, we highlight a newly observed confined random walk of the height of pressurized bulges and how temperature and gas-specific interactions influence the interfacial seal of the adhered films. While typically hydroscopic, and sensitive to ambient moisture, polyaramids in this 2D form of stacked platelets appear highly resistant to delamination and film decomposition.

Recent advances in optical interferometry and real-time monitoring capabilities[4,15] have elevated the bulge test to a dynamic platform for understanding the complex interplay between material properties, processing history, and interfacial phenomena that govern nanofilm performance. There are noted fluctuations in the literature of impermeable graphene bulges[13] which are not attributable to AFM measurement error and have yet to be explored. The dynamic adhesion of the nanofilm to the substrate, while studied as a mechanical property[16], has yet to be understood in context of

gas transport phenomena. This is a critical potential failure mode of the gas transport bulge test measurement, as gas may leak through the interface between the nanofilm and substrate. Interfacial leakage confounds permeability measurements through the film itself, which rely on the assumption of molecular transport occurring completely across the film area suspended over the microwell.

In general, 2D polymers show promise as novel gas membrane and barrier materials. As a class of materials, they combine the mechanical strength and in-plane energy conduction of conventional 2D materials[7,17–19] with the low densities, synthetic processability, and organic composition of traditional 1D polymers. Recent theoretical[20] and experimental[3] work has enabled the irreversible, solution-phase polymerization of 2D polyaramids. Using standard spin-coating procedures, 2D polyaramids have already achieved highly oriented, large area free-standing films which exhibit exceptional 2D elastic modulus and yield strength already reaching 12.7 GPa and 0.5 GPa, respectively[3]. These ultra-thin, high mechanical strength films have the potential to excel as gas membranes and/or barrier materials[21].

In this work, we study the behavior of 2DPA nanofilm bulges over 1000-days, and address questions relating to rim seal dynamics, bulge height fluctuations and adhesive stability. We also note the stability of such films to ambient humidity over extended durations. Furthermore, we analyze the impact of different environmental factors on the interfacial *rim seal* – defined as the seal made by the nanofilm along the circumference of the supporting well.

2. 2D Polyaramid System and Characterization

2D polymers have promising gas barrier and membrane applications due to their high processability and molecularly controllable pore size and overlap. 2DPA-1, or 2D polyaramid-1, shown to be molecularly impermeable to N_2 gas,[4] forms molecularly thin platelets concatenated with amide bonds, which, when spin-coated into nanofilms between 4 and 65nm in thickness, stack in such a way that any potential voids are inaccessible (*Figure 1A*). Using a wet-transfer process,[4] we have created a variety of samples for the bulge test measurement (*Figures 1B and 1C)*. Within this study, we used two types of lithographically etched silicon substrates: the first, Substrate I, has circular wells with depth to width ratios of 5:1 (98:14μm) and 7:1 (123:24 μm) and the second, Substrate II has depth to width ratios of 1:8.5 (1.0:8.5 μm). These different patterns affect the sensitivity of the bulge height to the net gas leak rate as it is inversely proportional to the well volume. We found that the substrates also had different rim seal adhesions, presumably due to processing conditions.

First, we discuss various characteristics of 2DPA-1 that support the stability and longevity of its impermeability properties. We found with density functional theory (DFT) calculations on bilayer configurations of 2DPA-1 with various interlayer offsets that the most minimum energy, stable configurations have staggered pores. For each offset, we first relaxed the system by performing a geometric optimization in vacuum using DFT. We computed the interlayer interaction energy, E_{int}, for the final optimized geometry using:

View Article Online
DOI: 10.1039/D5FD00034G

$$E_{\mathrm{int}} = E_{\mathrm{bl}} - E_{\mathrm{ml}-1} - E_{\mathrm{ml}-2} \qquad \text{Equation 1}$$

where E_{bl} is the energy of the bilayer and $E_{\mathrm{ml}-1}$ and $E_{\mathrm{ml}-2}$ are the energies of the two monolayers. Snapshots of the various bilayer configurations considered as well as the corresponding interlayer interaction energies are found in *Figure 1D*. We find that staggered pores have the most energetically favorable stacking configurations and that eclipsed stacking (i.e. AA stacking) are the least favored. There are numerous stacking configurations with varied pore-to-pore offsets that possess similarly favorable energies, indicating a tendency to stack in a variety of staggered configurations.

Another favorable property of 2DPA-1 is its environmental stability. In contrast to 1D polyaramids which are notoriously hygroscopic,[22–24] we show water to have no notable effect on the chemical or molecular structure of 2DPA-1 after 539 days, or approximately 1.5 years, of exposure (*Figure 1E*). We stored a 1:1 mass ratio of 2DPA-1 powder in DI water and compared the NMR spectra of the sample before and after the storage. We note that there is a slight increase in the r-value, or ratio of main-chain (H_A) to the end-group proton H_B,[25] from 5.15 to 5.45, as well as a decrease in the presence of sharp peaks in the main-chain and end-group proton regions (H_B, H_C, 1-5). These observations are consistent with a slight decrease in the presence of small molecular weight fragments, which could hydrolyze in water. The rate of such hydrolysis is expected to be slow at neutral pH because the amide carbonyl is poorly electrophilic, and water is a weak nucleophile. The amide resonance structure stabilizes the C–N bond, reducing susceptibility to rapid nucleophilic attack.[26,27] Over 18 months, a slow reaction at room temperature may reasonably increase the r value by 6% as observed. A more likely effect of water emersion is water intercolation and disruption of hydrogen bonding. This physical change in 2DPA material assembly not be immediately observable in H-NMR and r value but would impact the stability of a suspended nanofilm, as explored later in this work. In powder form, the experiment over 18 months confirms a lack of hygroscopic chemical degradation as expected.

3. Longitudinal Stability of 2DPA-1 Bulges

We generated a cohort of twenty-five 2DPA-1 bulges suspended over microwells and filled with air, and followed them over the course of more than 1000 days, or 3 years (*Figure 2A*). We transferred 2DPA-1 films ranging from 12.8 to 66 nm in thickness onto 8 different wafers with the pattern of Substrate I. These bulges exhibited unexpected stability with all bulges remaining upwardly deflected for the entire study range, invariant to changes in atmospheric temperature, pressure, or continuous exposure to

atmospheric humidity. We note that the initial heights of these samples are not equal and that, in general, bulges on the same substrate do not have equal initial heights.[4] We attribute this stochasticity to variations in the filling behavior. The opening of the rim seal is not currently controllable, leading to bulges that are sometimes adhered to the inside of the well to varying degrees.

We find that the AFM-measured deflections of the bulges show that bulges can increase or decrease between measurements on the order of tens of nanometers, and we show that this can be modelled by the confined diffusion of gas molecules within the bulges (*Figure 2B-2C*). Such fluctuations on the order of days are observable in other published data sets[13] but to our knowledge, studied here for the first time. We begin with an expression for the mean squared displacement (MSD):

$$MSD(t=\tau) = \frac{1}{N-\tau}\sum_{i=1}^{N-\tau} \|X_{i+\tau} - X_i\|^2 \qquad \text{Equation 2}$$

where X is the position vector of a molecule, N is the total number of molecules within the system, τ is an arbitrary time, and i is an integer. The MSD has different relationships with t dependent on the type of diffusion: linear indications Brownian motion, quadratic indicates Brownian motion with drift, and sublinear indicates confined diffusion. For confined diffusion,[28]

$$MSD\ (t) = \frac{L_c^2}{a}(1 - be^{-c\sigma^2 t/(2L_c^2)}) \qquad \text{Equation 3}$$

where L_c is a characteristic size of the region of confinement, a is a scaling parameter, b and c depend on the shape of the region, and σ is a constant diffusion coefficient. For our 25 2DPA-1 bulges measured over 3 years, we calculated the MSD over time (*Figure 2B*) and fit a scaling relationship, which was found to be an exponential plateau for all 25 bulges. We then extracted L_c from each of these fits and compared them to the corresponding bulge volume (*Figure 2C*), assuming the bulge approximates a circular paraboloid (*Figure S1*). We also analyzed and included 10 graphene bulges with diameters of 0.5 and 1.0 um from the literature[13] measured over 800 hours, or over 30 days, using mechanical properties from literature.[16,29] We find that the L_c corresponds to the bulge volume with R^2=0.95 and that this correlation holds when analyzing the different bulge materials and bulge diameters. This physical correlation is appropriate; the range of motion of the bulge should be determined by its initial volume, bounding the 1D random walk of the bulge height. We also find correlations between L_c and the initial bulge height, initial bulge surface area, and initial pressure difference across the bulge (*Figure S2*); however, these correlations have lower correlation coefficients.

There are subtle fluctuations in atmospheric temperature and pressure as well as environmental vibrations that the bulges may be subject to as they are stored and then transferred to the AFM, and these conditions may have a delayed impact on the bulges though latent adhesion mechanics. We rule out that fluctuations in temperature directly cause appreciable thermal expansions in the substrate, leading to these variations, by using known coefficients of thermal expansion for silicon and estimating sub-angstrom changes in the well diameters (*Equation S3*). Instead, we note that the temperature/pressure fluctuations would result in some change in the observed gas volume within the wells and thus the bulge height, and while the bulges correlate in their height fluctuations, there is a lack of correlation with ambient conditions (*Figure S3*), supporting the idea of mechanical or latent delay in effect. The bulge system is pushed upward by the encapsulating gas pressure but restrained by both the in-plane tension of the nanofilm and the van der Waals adhesion of the nanofilm to the wall. The dynamics of upward shock and downward restoration need not be matched. Such a mismatch would convert perturbative shocks from changes in temperature and vibration to fluctuations about an equilibrium height and allow the observations of the 1D random walk.

We also find that there are subtle fluctuations in the bulge diameters (±1μm) but similarly rule out the effect of these fluctuations on the bulge heights (*Figure S4*). These fluctuations can be attributed to measurement error and have no correlation between bulges on the same substrate or bulges measured on the same day.

We note that there exists a verification technique to show that these longitudinal bulges in fact retain gas and are not permeating throughout the study; this entails puncturing the bulges, such as with an AFM tip in *Contact Mode*, and observing its deflation. We have multiple examples of punctured bulges returning to their initial, un-inflated states (*Figure S5*); however, we do note that the type of puncture and amount of interaction between the AFM tip and bulge can affect the deflation dynamic (*Figure S5*). Given the destructive nature of this technique, we have sampled only a few but not all of the samples, showing that they can be punctured in this way.

4. Environmental Impact on Bulge Stability

Pressurization-Induced Rim Seal Opening Model

The persistence of a bulge, while attributable to the impermeability of the nanofilm, is also strongly coupled with the strength of the interfacial rim seal of each observed microwell – understanding the nature of the rim seal is crucial to repeatedly forming extremely stable bulges.

To understand further the behavior of the interfacial rim seal, we sought to model the gas-filling procedure of 2DPA-1 bulges with N_2. Bulge samples can controllably be made to have negative deflections by transferring 2DPA-1 films onto the substrates at elevated temperatures (50°C), and then made to have positive deflections by pressuring the sample at 150 kPa with N_2. Our analysis with an optical interferometry technique verifies that the bulge heights steadily increase throughout the filling.[4,15] Given 2DPA-1's

ultra-low permeability to N_2, we propose that N_2 enters the bulge through the interfacial rim seal.

We use a single point model, wherein the bulge is approximated as a cone with maximum deflection δ, in combination with the ideal gas law to validate the basic assumptions of these observations and our hypothesis. For this, we begin with a force balance on the conical bulge, normal to the top of the bulge:

$$\Sigma F_N = 0 \qquad \text{Equation 4}$$

$$P_{int} - P_{ext} - \frac{F_{spring}}{A_{well}} = 0 \qquad \text{Equation 5}$$

where P_{int} is the pressure internal to the bulge, P_{ext} is the pressure external to the bulge, and F_{spring} is the tension force within the bulge modelled as a Hookean spring. We use a modified spring constant, $\gamma = k/A$, and thus have the following pressure term for the bulge tension:

$$\frac{F_{spring}}{A_{bulge}} = \gamma(x - x_0)\frac{\delta}{x} \qquad \text{Equation 6}$$

where x is the extensional slant length of a cone, $\sqrt{r^2 + \delta^2}$, and x_0 is the extensional slant length of a cone at $r = 0$. During the initial transfer of the 2DPA-1 film onto the substrate at 50°C, we assume that the film is unstressed and flat and that $P_{int} = P_{ext} = 1$ atm, which thus gives us an initial condition to calculate γ, hence referred to as γ_1. We also assume an initial molar amount of internal gas, $n_{0,1}$. We now can apply our model to our experimentally monitored system wherein we used Substrate II (*Figure 3A*).

First, upon cooling to 25°C, we observe that the bulge becomes negatively deflected; this is reflected in the calculations when using γ_1, though the magnitudes are not equal (-380 nm experimentally, -709.6 nm theoretically). To rectify this, we thus calculate γ such that it results in them being equal, γ_2. Then, we pressurize the system to 2.48 atm using pure N_2. If the system is pressurized without any rim seal opening, using γ_2, we find that the film would touch the bottom of the well at around 1.8 atm, which would result in the film becoming irreversibly adhered via van der Waals forces. This counterfactual supports the observation that, instead, upon pressurization, the rim seal opens, allowing an inflow of N_2. Experimentally, we find that the bulge height reaches -200 nm during this pressurization and, when P_{ext} is reduced to 1 atm, the height rises to 225 nm. We calculate n_0 such that it would result in the height of -200 nm in the given conditions, $n_{0,2}$, and then compute that, upon pressure reduction to 1 atm, the height rises to 1110 nm. This accurately predicts the bulge's positive deflection, though it does overestimate the observation, and we can correct this by computing a new γ from experimental data, γ_3.

The one-point model is thus able to describe several bulge observations corresponding to before, during and after pressurization (*Figure 3B*). Overall, the model shows that the bulge behavior is consistent with the ideal gas law and a pressurized rim opening.

Faraday Discussions Accepted Manuscript Online
DOI: 10.1039/D6FD00034G

Gas-specific Effects

Gases including N_2, SF_6, Ar, and CH_4 have been shown to form 2DPA-1 bulges persisting for multiple days while gases including O_2, CO_2, He, and H_2 did not.[4] To elucidate the rim seal's potential contribution to permeance, we observed a system of N_2 filled bulges (24+ hours) exposed to He (35nm thick, r=9.18, Substrate II).

We found that persistent 2DPA-1 bulges filled with N_2 consistently deflated after exposure to He (*Figure 3C, 3D*), supporting the hypothesis that He molecules can alter the rim seal and affect the bulge test measurement. We began with 8 microwells, all initially downward deflected due to the annealing of the sample and pressurized them with 150 kPa of N_2 for 6 hours. The resulting samples were positively deflected and maintained this deflection for at least 24 hours, which is empirical evidence that they had an intact rim seal. Then, within an environmental chamber, we applied a gentle flow of He at near-atmospheric pressure, manually confirmed at the chamber outlet, across the bulges for 7 to 15 minutes (*Figure 3D i*). In a system with an intact rim seal, we anticipate that the He either permeates inside the well, increasing the heights, or does not permeate, leaving the heights unaffected. Using an algorithm based in interferometry that converts optical micrographs to height data,[4,15] we were able to convert the optical images of the bulges within this environmental chamber into height information and validate that all 8 bulges maintained their upward deflection during the He flow. However, after the He flow, the heights appear to slowly increase, and then, over the course of 24 hours, all 8 bulges were measured with an AFM to be downward deflected *(Figure 3D ii)*. Given that these bulges initially retained their rim seal during the N_2 pressurization and He flow, it is possible that the interaction of He with the film and substrate caused the rim seal to open, leading to this eventual bulge deflation. In all cases, the resulting downward deflected state was within 50nm of the initial state of these bulges, supporting that all the gas, including the nitrogen, had left the bulges.

Temperature Effects

To better understand the longitudinal stability of 2DPA-1 bulges, we studied the effects of temperature on its permeability and the ability to maintain the rim seal at elevated temperatures. This also elucidates the potential impact of physisorbed water molecules on the observed film impermeability. Using the Substrate II design, we measured the deflections within a temperature-controlled AFM of four 2DPA-1 bulges (35nm thick, r=9.67). We first increased the temperature from 35 to 80 to 120°C, then modulated it between 80 and 120°C.

We find that all 4 bulges exhibit the same behavior: initially decaying upon the first temperature increase, then oscillating between heights as the temperature is modulated (*Figure*

4A). None of the bulges completely deflated, which is what would be expected if physisorbed water contributed to the observed impermeability. We hypothesize that the initial decay is due to a temporary and reversible opening of the rim seal, likely owing to the influence of heating on the adhesion between the film and substrate. When subsequently oscillating the temperature between 80°C and 120°C for 2.5 cycles, the bulge deflections similarly oscillated on the order of 10 nm.

The diameters of all 4 bulges increase during the first temperature ramp, correlating to the observed bulge deflation (Figure 4B). 3 of the bulges exhibit the diameter increase at the first temperature increase (Figures 4B i, ii, iv) while the fourth does so at an approximately 15-minute delay (Figure 4B iii). The rim seal thus appears to have some stochasticity to its behavior. Then, the diameters either decrease or stay approximately constant, with variations that could be attributed to measurement error. This corresponds to the hypothesis that the rim seal closes after the initial temperature increases. We can characterize the adhesion energy between the film and the substrate based on the initial diameter increase, assuming that this delamination is driven by pressure increases:[30]

$$\Gamma = \frac{5C}{4}\left(p_0 \frac{V_0}{V_0+V_B(a)} - p_{\text{ext}}\right)\delta \qquad \text{Equation 7}$$

where Γ is the adhesion energy, p_0 is the internal pressure of the bulge, V_0 is the initial volume of microwell, V_B is the volume of the nanofilm bulge as a function of the bulge radius a, p_{ext} is the external (atmospheric) pressure, and C is a constant based on Poisson's ratio. Because this analysis does not consider temperature effects on the van der Waals forces between the film and substrate, we consider this quantitative analysis as a lower bound estimation of the surface adhesion energy. We find the adhesion energies to be 0.019, 0.014, 0.022, and 0.017 J/m^2. We previously reported an adhesion energy, calculated for a flat 2DPA-1 thin film, of 0.29 J/m^2, which is an overestimation of a bulged 2DPA-1 thin film's adhesion energy.[31] We therefore conclude that the true value of the surface energy can be bounded by the values we provide here and the values calculated for a flat film.

At the elevated temperatures of 80 and 120°C, we propose that the bulges maintain their impermeability, the rim seal is still intact, and the gas within the well is expanding its volume in agreement with the ideal gas law. To quantify this, we begin with using the ideal gas law to relate the bulge state at 80°C to 120°C, assuming no permeation:

$$\frac{P_1V_1}{T_1} = \frac{P_2V_2}{T_2} \qquad \text{Equation 8}$$

Then, we insert an expression for the well volume, assuming that the bulge approximates a circular paraboloid ($V = \pi r^2 L + \pi r^2\delta/2$), and insert Hencky's solution[32] as the expression for pressure, as this model accounts for material properties such as the elastic modulus. This yields:

View Article Online
DOI: 10.1039/D6FD00034G

$$\frac{\frac{(A\delta_1^3+B\delta_1+P_{atm})(2\pi rL+\pi r^2\delta_1/2)}{T_1}}{\frac{(A\delta_2^3+B\delta_2+P_{atm})(2\pi rL+\pi r^2\delta_2/2)}{T_2}} = \qquad \text{Equation 9}$$

where A and B are constants within Hencky's solution dependent on material properties. Thus, for a given T_1, T_2, and δ_1, one can calculate δ_2.

Using the average experimental height at 80°C for each of the bulges, we calculated what the corresponding height should be at 120°C (*Figure 4C*). We calculated this using the mean of experimentally reported elastic moduli for 2DPA-1[3]. We find that the percent error between the theoretical and experimental bulge heights at 120°C range from 0.2% to 13.6%; per bulge, the average percent error is 4.1% (*Figure 4C i*), 7.4% (*Figure 4C ii*), 6.7% (*Figure 4C iii*), and 3.7% (*Figure 4C iv*). Hence, our results do not indicate any discernable gas loss while oscillating between 80 and 120 °C and supports the notion that physisorbed water cannot be the mechanistic explanation for the film's measured impermeability. In conjunction with the 1000-day data set, the impermeability properties of 2DPA-1 are unaffected by modulations in atmospheric humidity.

5. Conclusions

In this study, we present the first comprehensive framework for understanding long-term stability mechanisms in nanoscale thin film bulge test systems through an unprecedented 1000-day monitoring of 2DPA-1 microwells. The molecular-level packing architecture of 2DPA-1, validated through computational modeling, provides the fundamental basis for sustained impermeability across multiple environmental conditions. Our confined diffusion model successfully explains daily height fluctuations as intrinsic gas molecule dynamics rather than measurement artifacts, with characteristic length scales directly correlating to bulge geometry ($R^2 > 0.96$ for volume correlation). We demonstrate temperature-independent rim seal integrity up to 120°C through thermodynamic validation, while revealing critical gas-specific failure mechanisms that establish clear operational boundaries.

This mechanistic framework enables expansion of bulge test methodology to emerging nanomaterials systems where long-term reliability is paramount. The findings discussed here will guide the design of next-generation membrane materials and provide insight for assessing new material systems under realistic operating conditions.

6. Methods

Sample preparation

We transferred 2DPA-1 thin films onto the wafers using polystyrene (PS) as a sacrificial support layer. Silicon/silicon oxide (Si/SiO_2) wafers were sequentially sonicated in

View Article Online
DOI: 10.1039/D6FD00034G

acetone, then isopropanol for 5 minutes each, and dried with nitrogen gas. Then, 10 wt% PS dissolved in anisole was spin-coated onto the cleaned Si/SiO_2 substrates at 2000 rpm for 60 seconds. The PS-coated substrates were immediately transferred to a 110°C hotplate to anneal for 15 minutes under a glass cover to prevent contamination during solvent removal. Subsequently, 2DPA-1 solutions in trifluoroacetic acid (TFA) were spin-coated using identical parameters (2000 rpm, 60 seconds) onto the PS layer. Film thickness was controlled by varying the 2DPA-1 concentration in TFA. Following deposition, samples underwent brief thermal treatment at 50°C for 5 minutes to eliminate residual TFA, with non-uniform film edges trimmed to ensure thickness uniformity.

Then, we transferred the PS-supported 2DPA-1 films onto the etched substrates via wet-transfer. Using a razor blade, we excised sections of the films and floated them on DI water such that the 2DPA-1 layer faced upward. Etched substrates brought into contact with the 2DPA-1 surface, oriented so that the 2DPA-1 contacted the substrates, and carefully lifted from the water. Film-covered substrates were dried overnight at ambient conditions, with substrates requiring downward-deflected films annealed at 50°C during the drying process.

Following transfer, PS was dissolved away with sequential solvent treatments: initial exposure to 20 mL of 25% v/v chloroform in hexane for 4 hours, followed by 20 mL of 30% v/v chloroform in hexane for an additional 4 hours. Substrates were gently rinsed with hexane and air-dried to remove residual solvents. Completed 2DPA-1-coated substrates were stored under ambient laboratory conditions.

Bulge samples were prepared by initially creating downward-deflected membranes through controlled evacuation, followed by nitrogen pressurization at 300 kPa for 6 hours to create upward-deflected bulges. The pressurization chamber was maintained at room temperature with humidity control during sample preparation.

1H-NMR Characterization

We first prepared samples by suspending 2DPA-1 powders in deuterated trifluoracetic acid at a concentration of 10 mg mL^{-1}. We sonicated the solution in a BRANSON Ultrasonic Cleaner for 15 min before adding into a WILMAD NMR tubes (5 mm diam., economy). All the ^1H NMR measurements were performed at room temperature on an Avance III HD 500 NMR Bruker spectrometer.

Atomic Force Microscopy

To measure the deflections of bulge test samples, we used a Cypher S in tapping mode with an AC240 tip. We use a setpoint of 800 mV, scan rate of 1.5 Hz, a scan area of 20μm, and a resolution of 256x256 points and lines. Each bulge on the substrates is 8.5μm in diameter. For the temperature-controlled measurements, we used the heating stage attachment on a Cypher ES and the same parameters as above. For the puncture experiments, we used a Cypher S in contact mode.

7. References

(1) Colson, J. W.; Dichtel, W. R. Rationally Synthesized Two-Dimensional Polymers. *Nat. Chem.* **2013**, *5* (6), 453–465. https://doi.org/10.1038/nchem.1628.

(2) Payamyar, P.; King, B. T.; Öttinger, H. C.; Schlüter, A. D. Two-Dimensional Polymers: Concepts and Perspectives. *Chem. Commun.* **2015**, *52* (1), 18–34. https://doi.org/10.1039/C5CC07381B.

(3) Zeng, Y.; Gordiichuk, P.; Ichihara, T.; Zhang, G.; Sandoz-Rosado, E.; Wetzel, E. D.; Tresback, J.; Yang, J.; Kozawa, D.; Yang, Z.; Kuehne, M.; Quien, M.; Yuan, Z.; Gong, X.; He, G.; Lundberg, D. J.; Liu, P.; Liu, A. T.; Yang, J. F.; Kulik, H. J.; Strano, M. S. Irreversible Synthesis of an Ultrastrong Two-Dimensional Polymeric Material. *Nature* **2022**, *602* (7895), 91–95. https://doi.org/10.1038/s41586-021-04296-3.

(4) Ritt, C. L.; Quien, M.; Wei, Z.; Gress, H.; Dronadula, M.; Altmisdort, K.; Tu, Y.-M.; Gadaloff, M.; Aluru, N. R.; Ekinci, K. L.; Bunch, J. S.; Strano, M. S. A Molecularly Impermeable Polymer from Two-Dimensional Polyaramids. ChemRxiv October 17, 2024. https://doi.org/10.26434/chemrxiv-2024-c8b17-v2.

(5) Akinwande, D.; Brennan, C. J.; Bunch, J. S.; Egberts, P.; Felts, J. R.; Gao, H.; Huang, R.; Kim, J.-S.; Li, T.; Li, Y.; Liechti, K. M.; Lu, N.; Park, H. S.; Reed, E. J.; Wang, P.; Yakobson, B. I.; Zhang, T.; Zhang, Y.-W.; Zhou, Y.; Zhu, Y. A Review on Mechanics and Mechanical Properties of 2D Materials—Graphene and Beyond. *Extreme Mech. Lett.* **2017**, *13*, 42–77. https://doi.org/10.1016/j.eml.2017.01.008.

(6) Cooper, R. C.; Lee, C.; Marianetti, C. A.; Wei, X.; Hone, J.; Kysar, J. W. Nonlinear Elastic Behavior of Two-Dimensional Molybdenum Disulfide. *Phys. Rev. B* **2013**, *87* (3), 035423. https://doi.org/10.1103/PhysRevB.87.035423.

(7) Lee, C.; Wei, X.; Kysar, J. W.; Hone, J. Measurement of the Elastic Properties and Intrinsic Strength of Monolayer Graphene. *Science* **2008**, *321* (5887), 385–388. https://doi.org/10.1126/science.1157996.

(8) Castellanos-Gomez, A.; Poot, M.; Steele, G. A.; van der Zant, H. S. J.; Agraït, N.; Rubio-Bollinger, G. Elastic Properties of Freely Suspended MoS2 Nanosheets. *Adv. Mater.* **2012**, *24* (6), 772–775. https://doi.org/10.1002/adma.201103965.

(9) Banhart, F.; Kotakoski, J.; Krasheninnikov, A. V. Structural Defects in Graphene. *ACS Nano* **2011**, *5* (1), 26–41. https://doi.org/10.1021/nn102598m.

(10) Bunch, J. S.; Verbridge, S. S.; Alden, J. S.; van der Zande, A. M.; Parpia, J. M.; Craighead, H. G.; McEuen, P. L. Impermeable Atomic Membranes from Graphene Sheets. *Nano Lett.* **2008**, *8* (8), 2458–2462. https://doi.org/10.1021/nl801457b.

(11) Wang, L.; Drahushuk, L. W.; Cantley, L.; Koenig, S. P.; Liu, X.; Pellegrino, J.; Strano, M. S.; Scott Bunch, J. Molecular Valves for Controlling Gas Phase Transport Made from Discrete Ångström-Sized Pores in Graphene. *Nat. Nanotechnol.* **2015**, *10* (9), 785–790. https://doi.org/10.1038/nnano.2015.158.

(12) Drahushuk, L. W.; Wang, L.; Koenig, S. P.; Bunch, J. S.; Strano, M. S. Analysis of Time-Varying, Stochastic Gas Transport through Graphene Membranes. *ACS Nano* **2016**, *10* (1), 786–795. https://doi.org/10.1021/acsnano.5b05870.

(13) Sun, P. Z.; Yang, Q.; Kuang, W. J.; Stebunov, Y. V.; Xiong, W. Q.; Yu, J.; Nair, R. R.; Katsnelson, M. I.; Yuan, S. J.; Grigorieva, I. V.; Lozada-Hidalgo, M.; Wang, F. C.; Geim, A. K. Limits on Gas Impermeability of Graphene. *Nature* **2020**, *579* (7798), 229–232. https://doi.org/10.1038/s41586-020-2070-x.

(14) Berry, V. Impermeability of Graphene and Its Applications. *Carbon* **2013**, *62*, 1–10. https://doi.org/10.1016/j.carbon.2013.05.052.

(15) Quien, M.; Ritt, C. L.; Garimella, S. S.; Gress, H.; Ekinci, K. L.; Bunch, J. S.; Strano, M. S. Interferometric Deflection Analysis of Suspended 2D Polyaramid Thin Films. *Small Methods n/a* (n/a), e01543. https://doi.org/10.1002/smtd.202501543.

(16) Koenig, S. P.; Boddeti, N. G.; Dunn, M. L.; Bunch, J. S. Ultrastrong Adhesion of Graphene Membranes. *Nat. Nanotechnol.* **2011**, *6* (9), 543–546. https://doi.org/10.1038/nnano.2011.123.

(17) Pop, E.; Varshney, V.; Roy, A. K. Thermal Properties of Graphene: Fundamentals and Applications. *MRS Bull.* **2012**, *37* (12), 1273–1281. https://doi.org/10.1557/mrs.2012.203.

(18) Sandoz-Rosado, E.; Beaudet, T. D.; Andzelm, J. W.; Wetzel, E. D. High Strength Films from Oriented, Hydrogen-Bonded "Graphamid" 2D Polymer Molecular Ensembles. *Sci. Rep.* **2018**, *8* (1), 3708. https://doi.org/10.1038/s41598-018-22011-7.

(19) Sandoz-Rosado, E.; Beaudet, T. D.; Balu, R.; Wetzel, E. D. Designing Molecular Structure to Achieve Ductile Fracture Behavior in a Stiff and Strong 2D Polymer, "Graphylene." *Nanoscale* **2016**, *8* (21), 10947–10955. https://doi.org/10.1039/C5NR07742G.

(20) Zhang, G.; Zeng, Y.; Gordiichuk, P.; Strano, M. S. Chemical Kinetic Mechanisms and Scaling of Two-Dimensional Polymers via Irreversible Solution-Phase Reactions. *J. Chem. Phys.* **2021**, *154* (19), 194901. https://doi.org/10.1063/5.0044050.

(21) Luque-Alled, J. M.; Moreno, C.; Gorgojo, P. Two-Dimensional Materials for Gas Separation Membranes. *Curr. Opin. Chem. Eng.* **2023**, *39*, 100901. https://doi.org/10.1016/j.coche.2023.100901.

(22) Akay, M.; Ah Mun, S. K.; Stanley, A. Influence of Moisture on the Thermal and Mechanical Properties of Autoclaved and Oven-Cured Kevlar-49/Epoxy Laminates. *Compos. Sci. Technol.* **1997**, *57* (5), 565–571. https://doi.org/10.1016/S0266-3538(97)00017-1.

(23) Gavara, R.; Hernandez, R. J. The Effect of Water on the Transport of Oxygen through Nylon-6 Films. *J. Polym. Sci. Part B Polym. Phys.* **1994**, *32* (14), 2375–2382. https://doi.org/10.1002/polb.1994.090321408.

(24) Venoor, V.; Park, J. H.; Kazmer, D. O.; Sobkowicz, M. J. Understanding the Effect of Water in Polyamides: A Review. *Polym. Rev.* **2021**, *61* (3), 598–645. https://doi.org/10.1080/15583724.2020.1855196.

(25) Wei, Z.; Tu, Y.-M.; Yim, W.; Quien, M.; Alizadehmojarad, A. A.; Gong, X.; Strano, M. S. 1H NMR Trajectories for Analyzing the Growth and Purification of 2D Polyaramids. *J. Am. Chem. Soc.* **2025**, *147* (7), 5921–5932. https://doi.org/10.1021/jacs.4c15053.

(26) Xiong, W.; Wang, Y.; Yang, X.; Liu, W. H. Selective Hydrolysis of Primary and Secondary Amides Enabled by Visible Light. *Org. Lett.* **2023**, *25* (17), 2948–2952. https://doi.org/10.1021/acs.orglett.3c00354.

(27) *On the hydrolysis mechanisms of amides and peptides - East - 2018 - International Journal of Chemical Kinetics - Wiley Online Library*. https://onlinelibrary-wiley-com.libproxy.mit.edu/doi/full/10.1002/kin.21194 (accessed 2026-02-24).

(28) Briane, V.; Vimond, M.; Kervrann, C. An Overview of Diffusion Models for Intracellular Dynamics Analysis. *Brief. Bioinform.* **2020**, *21* (4), 1136–1150. https://doi.org/10.1093/bib/bbz052.

(29) Sun, P. Z.; Yang, Q.; Kuang, W. J.; Stebunov, Y. V.; Xiong, W. Q.; Yu, J.; Nair, R. R.; Katsnelson, M. I.; Yuan, S. J.; Grigorieva, I. V.; Lozada-Hidalgo, M.; Wang, F. C.; Geim, A. K. Limits on Gas Impermeability of Graphene. *Nature* **2020**, *579* (7798), 229–232. https://doi.org/10.1038/s41586-020-2070-x.

(30) Koenig, S. P.; Boddeti, N. G.; Dunn, M. L.; Bunch, J. S. Ultrastrong Adhesion of Graphene Membranes. *Nat. Nanotechnol.* **2011**, *6* (9), 543–546. https://doi.org/10.1038/nnano.2011.123.

(31) Gress, H.; Ritt, C. L.; Shomakhov, I.; Altmisdort, K.; Quien, M.; Wei, Z.; Lawall, J. R.; Boddeti, N.;

Strano, M. S.; Bunch, J. S.; Ekinci, K. L. Molecularly Thin Polyaramid Nanomechanical Resonators. *Nano Lett.* **2025**, *25* (50), 17301–17307. https://doi.org/10.1021/acs.nanolett.5c04440.

(32) H. Hencky. Uber den Spannungszustand in kreisrunden Platten mit verschwindender Biegungssteifigkeit. *Z. Math. Phys.* **1915**, *63*, 311–317.

View Article Online
DOI: 10.1039/D5FD00034G

View Article Online
DOI: 10.1039/D6FD00034G

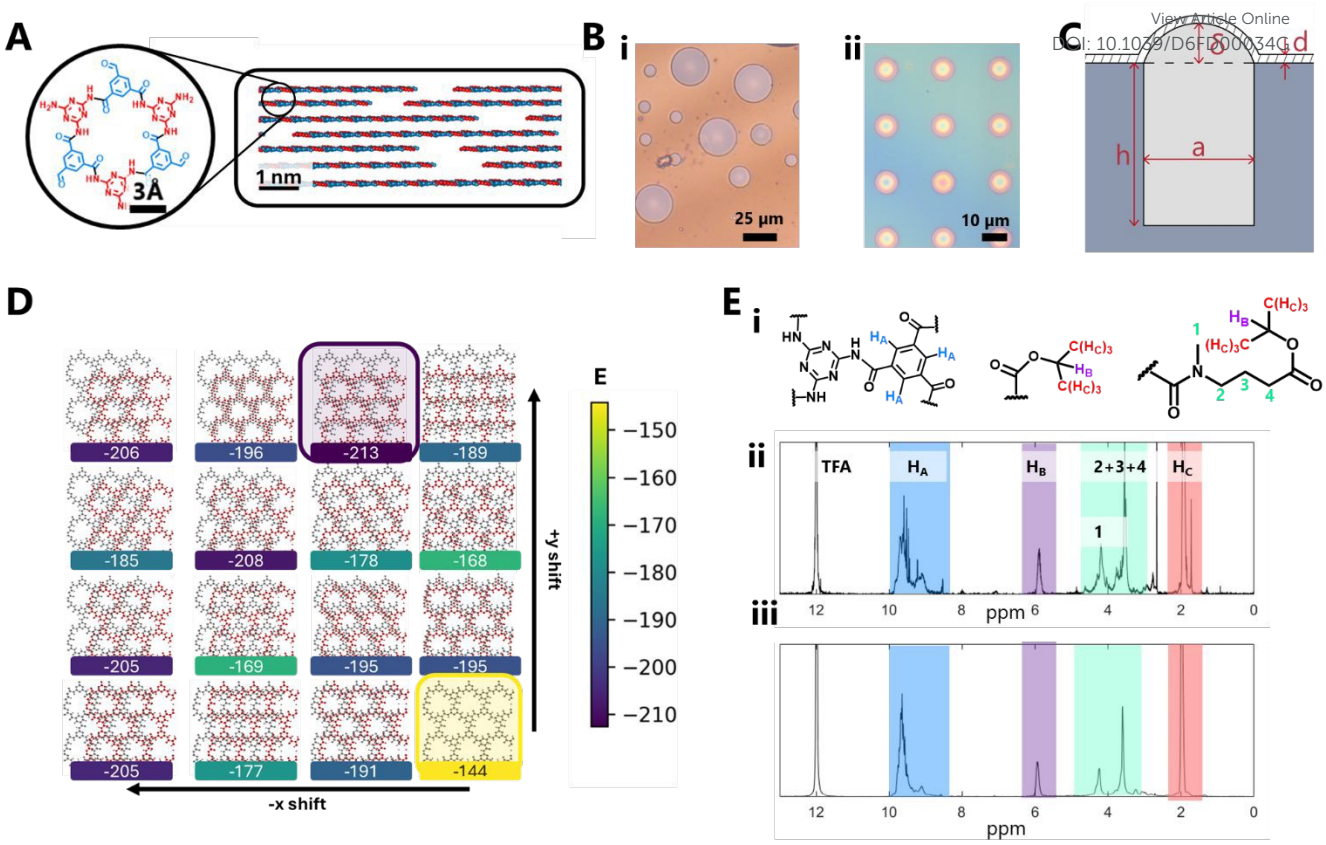

Figure 1.

A. Oligomer unit of 2DPA-1 with one pristine nanopore, inset with the side-view of a planar stack of seven 2DPA-1 layers with 0.36 nm interlayer spacing
B. Optical micrographs of substrates covered with 2DPA-1 thin films with patterned wells used for this study. Substrate (i) contains wells ranging from 5 to 14 to 24 um in diameter and 73 to 98 to 123 um in depth, respectively. Substrate (ii) contains wells that are 8.5um in diameter and 1um in depth.
C. Side-view schematic of bulge formation with trapped gas (light gray) from a 2DPA-1 film (hatch filled) transferred onto a silicon wafer (blue gray) with pre-patterned, cylindrical wells. A gap between the film and wafer is exaggerated to depict potential gas transfer through the rim seal. Relevant parameters are indicated on the schematic.
D. Snapshots of various bilayer offsets and their interaction energies determined from density functional theory (DFT) calculations. The configurations with the minimum and maximum energies are highlighted.
E. (i) Different protons within the 2DPA-1 structure, corresponding to the aromatic hydrogen on the main chain (H_A, blue), the hydrogen on the end groups quenched with IPA (H_B, purple), and the methyl hydrogen on the end groups quenched with IPA (H_C, red). (ii, iii) 1H-NMR spectroscopy of 2DPA-1 powder before (ii) and after (iii) being suspended in 1:1 mass ratio of water for 1.5 years. The different colored regions correspond to the same colored protons labelled in (i); acetone is present in (ii) around 2.8 ppm.

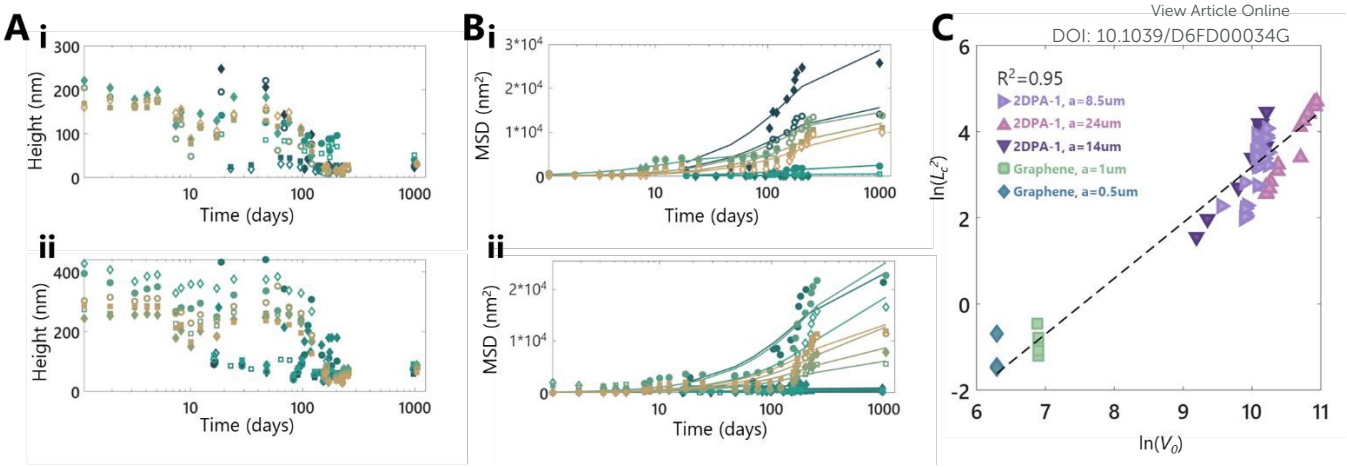

Figure 2.

A. Height extrema of 10 2DPA-1 bulges suspended over 14um diameter wells (i) and 15 2DPA-1 bulges suspended over 24um diameter wells (ii) over the course of more than 1000 days.
B. Mean square displacement (MSD) analysis of 2DPA-1 bulges over 14um (i) and 24um (ii) diameter wells wherein the solid lines are the fit results that have an optimized confinement length, L_c^2
C. Comparisons of ln (L_c^2), for graphene bulges (green square: a=1μm; blue diamond: a=0.5μm) and 2DPA-1 bulges (left pointing triangle: a=8.5μm; upwards pointing triangle: a=24μm; downwards pointing triangle: a=14μm) with logarithm of initial volume, V_0

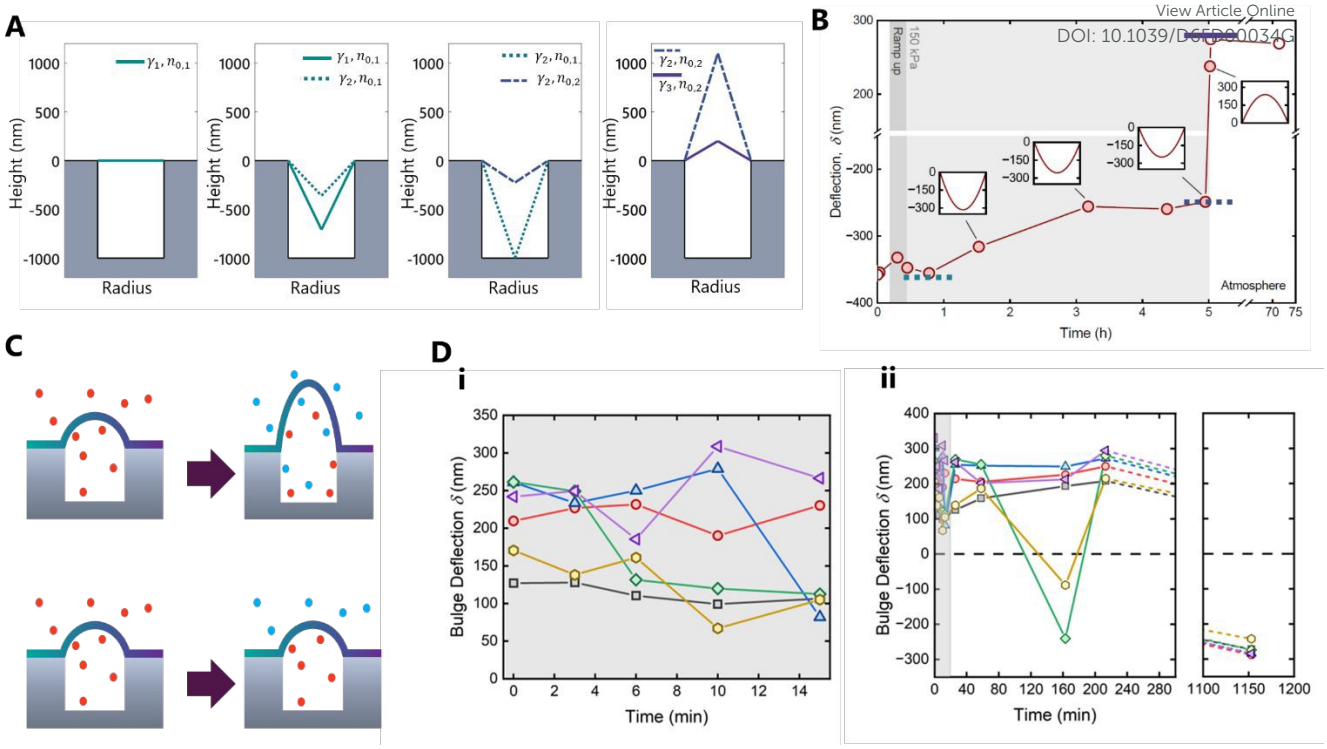

Figure 3.
A. Nitrogen pressurization process of 2DPA-1 bulges, where sequentially the external pressure and temperature are modulated to induce bulge filling, shown with the one-point cone model. Different line types denote the cone model results with different γ and n_o
B. Comparison of the one-point cone model results with experimental deflection data during nitrogen pressurization. Reproduced with permission from Ritt, Quien, Wei et al.[4]
C. Schematic of the helium experiment, wherein bulges prefilled with N2 (red circles) are subjected to helium gas (blue circles) of negligible pressure. If permeable, the bulges should increase in height (top), whereas if impermeable the bulges should not change in height (bottom).
D. Results of the full pressurization experiment with nitrogen, then helium, on 6 studied bulges (35nm thick, r=9.18). i) Change in height, determined interferometrically, during the He flow (gray box). ii) Change in height, determined interferometrically and with AFM, over entire measurement time with He flow in gray.

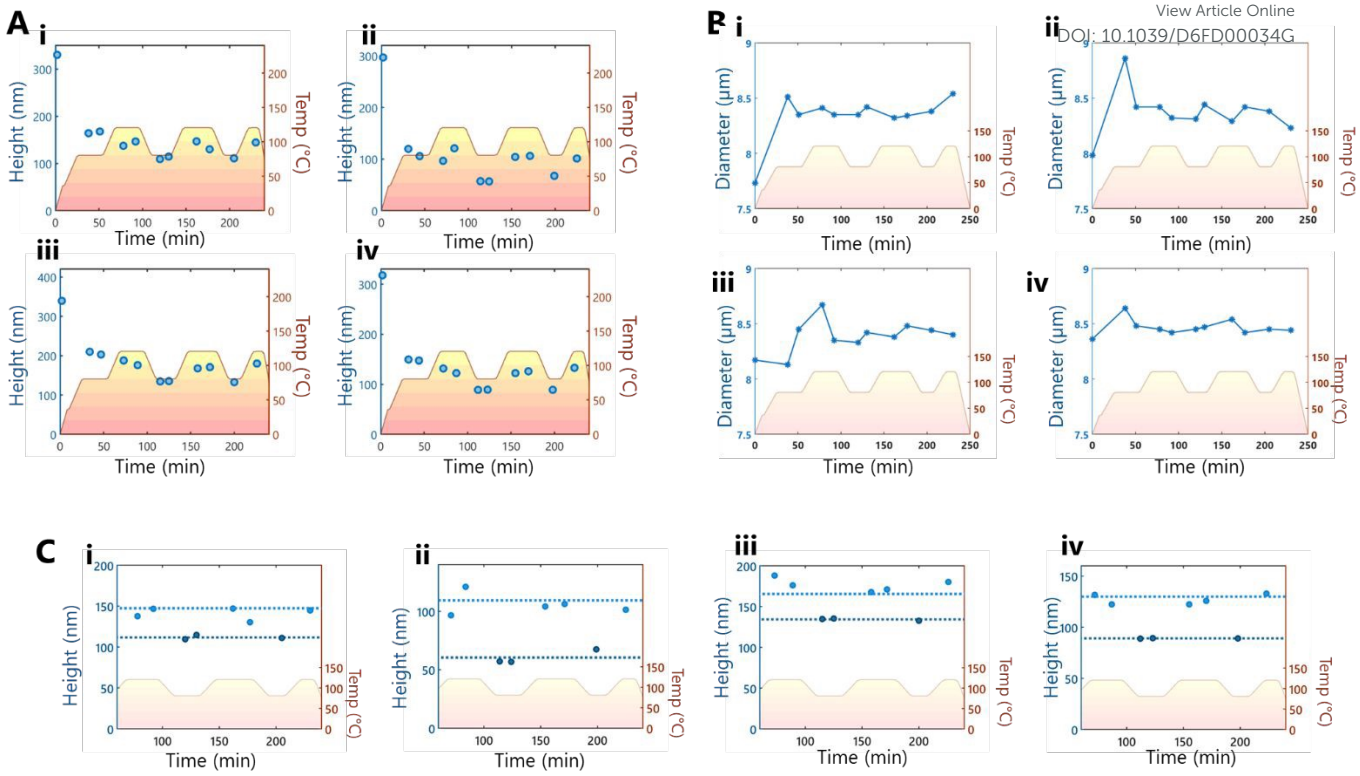

Figure 4.

A. AFM height extrema of each bulge (35nm thick, r=9.67) throughout the experiment (blue circles) with the temperature profile inset (red-yellow gradient)
B. Change in bulge diameter (blue asterisk) throughout the experiment. Temperature profile is inset along the bottom (red-yellow gradient).
C. Comparison of the theoretical height of an impermeable bulge at 120C (light blue dashed line), calculated using the average experimental height at 80C (dark blue dashed line), with the experimental data points at 80 C (dark blue circles) and 120 C (light blue circles). Temperature profile is inset along the bottom (red-yellow gradient).

View Article Online
DOI: 10.1039/D6FD00034G

View Article Online
DOI: 10.1039/D6FD00034G

The datasets generated during and/or analyzed during the current study are available from the authors upon request.